QCD equation of state for heavy ion collisions[*]

A-Meng Zhao(赵阿蒙)[1;1)]   Yuan-Mei Shi(石远美)[2,4]   Jian-Feng Li(李剑锋)[3,4]   Hong-Shi Zong(宗红石)[4,5,6;2)]

[1] Department of Foundation, Southeast University Chengxian College, Nanjing 210088, China
[2] Department of Physics and Electronic Engineering, Nanjing Xiaozhuang University, Nanjing 211171, China
[3] College of Mathematics and Physics, Nantong University, Nantong 226019, China
[4] Department of Physics, Nanjing University, Nanjing 210093, China
[5] Joint Center for Particle, Nuclear Physics and Cosmology, Nanjing 210093, China
[6] State Key Laboratory of Theoretical Physics, Institute of Theoretical Physics, CAS, Beijing 100190, China

Abstract: In this work, we calculate the equation of state (EoS) of quark gluon-plasma (QGP) using the Cornwall-Jackiw-Tomboulis (CJT) effective action. We get the quark propagator by using the rank-1 separable model within the framework of the Dyson-Schwinger equations (DSEs). The results from CJT effective action are compared with lattice QCD data. We find that, when μ is small, our results generally fit the lattice QCD data when $T > T_c$, but show deviations at and below T_c. It can be concluded that the EoS of CJT is reliable when $T > T_c$. Then, by adopting the hydrodynamic code UVH2+1, we compare the CJT results of the multiplicity and elliptic flow v_2 with the PHENIX data and the results from the original EoS in UVH2+1. While the CJT results of multiplicities generally match the original UVH2+1 results and fit the experimental data, the CJT results of v_2 are slightly larger than the original UVH2+1 results for centralities smaller than 40% and smaller than the original UVH2+1 results for higher centralities.

Keywords: heavy ion collisions, equation of state, multiplicity, elliptic flow, CJT effective action

PACS: 12.38.Lg, 11.10.Wx, 12.38.Mh   **DOI:** 10.1088/1674-1137/41/10/103101

1   Introduction

Quantum chromodynamics (QCD) is the fundamental theory of the strong interaction. Heavy ion collisions are important experiments to test the theory. We attempt to use the Dyson-Schwinger equations and Cornwall-Jackiw-Tomboulis (CJT) effective action to analyze heavy ion collisions. By doing this, we can deepen our understanding of QCD theory as well as of heavy ion collisions.

The equation of state (EoS) plays an important role in studying the quark-gluon plasma (QGP) [1] created in relativistic heavy ion collisions. In QGP the temperature (T) and chemical potential (μ) are non-zero at the same time. It should be emphasized that compared with temperature, the quark chemical potential μ is small for QGP created in relativistic heavy ion collisions. For example, at $\sqrt{S_{NN}}$=200 GeV in RHIC, μ is about 9 MeV, and for the heavy ion collisions in the LHC, μ is even smaller. When we try to get the EoS of QGP created in RHIC and the LHC, these properties should be considered.

By generalizing CJT effective action [2, 3] to the condition of finite temperature and chemical potential, the EoS of QGP can be obtained. Some previous works in this area include studies on partition function [4, 5], the pressure difference between the Nambu-Goldstone phase and the Wigner phase [6], and so on.

Since CJT effective action is decided by the quark propagators (free and dressed), the equation of state from QCD relies on a reliable quark propagator only. In this paper we adopt the dressed quark propagator from the rank-1 separable model of the Dyson-Schwinger equation method. This model is found to be successful in describing light flavor pseudoscalar and vector meson observables [7]. In Refs. [8, 9] it is used to calculate the susceptibilities of quark-number.

When we obtain the EoS of QGP, we can describe its evolution by relativistic hydrodynamics. Here we adopt UVH2+1 (UVH2+1-0.0beta) [10–13], a dissipative hydrodynamic model, that constructs the dissipative part of the stress-energy tensor, $\Pi_{\mu\nu}$, in the framework of the

Müller-Israel-Stewart theory. Then we can get some physics observables and compare them with the experimental data. Here we choose the multiplicity of produced particles and the elliptic flow for comparison.

2 QCD EoS from CJT effective action and thermal self-consistency

The pressure from CJT effective action is [2–5]:

$$
P_{\mathrm{CJT}}(T,\mu) = \frac{T}{V}\ln Z_{\mathrm{CJT}}(T,\mu)
$$

$$
= -N_{\mathrm{c}}N_{\mathrm{f}}T\sum_{k=-\infty}^{+\infty}\int\frac{\mathrm{d}^3p}{(2\pi)^3}\mathrm{tr}[\ln(G^{-1}(\widetilde{p}_k)G_0(\widetilde{p}_k))
$$

$$
-\frac{1}{2}(1-G_0^{-1}(\widetilde{p}_k)G(\widetilde{p}_k))] \;, \tag{1}
$$

where μ is the chemical potential of the quarks ($\mu=\mu_{\mathrm{u}}=\mu_{\mathrm{d}}=\frac{1}{3}\mu_{\mathrm{B}}$), and $\widetilde{p}_k=(\vec{p},\widetilde{\omega})=(\vec{p},i\mu+\omega_k)$, $\omega_k=(2k+1)\pi T$ the fermion Matsubara frequencies.

When the temperature is high enough, the quark propagator comes back to its free form $G\to G_0$, so that the pressure is also back to its free form $P(T,\mu)\to P_{\mathrm{free}}(T,\mu)$. The pressure of a free gas consisting of massless quarks, anti-quarks and gluons at fixed T and μ is [1]:

$$
P_{\mathrm{free}}(T,\mu)=\frac{37\pi^2}{90}T^4+\mu^2T^2+\frac{\mu^4}{2\pi^2}-\mathcal{B} \;. \tag{2}
$$

The bag constant $\mathcal{B}$ is thought of as a measure of the energy density of the vacuum. But when $G\to G_0$, it is found that Eq. (1) is equal to zero. To make a correction, we can define (some similar arguments exist in Ref. [5]):

$$
P(T,\mu) = \frac{T}{V}\ln Z(T,\mu)=P_{\mathrm{CJT}}(T,\mu)+P_{\mathrm{free}}(T,\mu)
$$

$$
= -N_{\mathrm{c}}N_{\mathrm{f}}T\sum_{n=-\infty}^{+\infty}\int\frac{\mathrm{d}^3p}{(2\pi)^3}\mathrm{tr}\Big[\ln(G^{-1}(\widetilde{p}_k)G_0(\widetilde{p}_k))
$$

$$
-\frac{1}{2}(1-G_0^{-1}(\widetilde{p}_k)G(\widetilde{p}_k))\Big]
$$

$$
+\frac{37\pi^2}{90}T^4+\mu^2T^2+\frac{\mu^4}{2\pi^2}-\mathcal{B} \;. \tag{3}
$$

Since $\partial P_{\mathrm{free}}/\partial G=0$, this correction will not break the self-consistency of CJT.

The quark propagator under the rainbow approximation of the Dyson-Schwinger equations, at finite T and μ, reads [6, 8, 14]:

$$
G^{-1}(\widetilde{p}_k)=
$$

$$
\mathrm{i}\gamma\cdot\widetilde{p}_k+m+\frac{4}{3}T\sum_{i=-\infty}^{+\infty}\int\frac{\mathrm{d}^3q}{(2\pi)^3}g^2D_{\mu\nu}^{\mathrm{eff}}(\widetilde{p}_k-\widetilde{q}_n)\gamma_\mu G(\widetilde{q}_n)\gamma_\nu \;. \tag{4}
$$

Here we adopt the rank-1 separable model. The gluon propagator is as proposed in Refs. [7, 15]:

$$
g^2D_{\mu\nu}^{\mathrm{eff}}(\widetilde{p}_k-\widetilde{q}_n)=\delta_{\mu\nu}D_0f_0(\widetilde{p}_k^2)f_0(\widetilde{q}_k^2) \;, \tag{5}
$$

where $f_0(\widetilde{p}_k^2)=\exp(-\widetilde{p}_k^2/\Lambda^2)$, with $\Lambda=0.678$ GeV, $D_0\Lambda^2=128.0$ and the degenerate light quark mass $m=6.6$ MeV [7]. These parameters are found to be successful in describing light flavor pseudoscalar and vector meson observables.

At the same time, the quark propagator is generally decomposed as

$$
G^{-1}(\widetilde{p}_k)=\mathrm{i}\vec{\gamma}\cdot\vec{p}A(\widetilde{p}_k^2)+\mathrm{i}\gamma_4\widetilde{\omega}_kC(\widetilde{p}_k^2)+B(\widetilde{p}_k^2) \;. \tag{6}
$$

For the rank-1 separable model, the rainbow-DSE solution is $A(\widetilde{p}_k^2)=C(\widetilde{p}_k^2)=1$ and $B(\widetilde{p}_k^2)=m+b(T,\mu)f_0(\widetilde{p}_k^2)$, where

$$
b(T,\mu)=\frac{16}{3}D_0T\sum_{n=-\infty}^{+\infty}\int\frac{\mathrm{d}^3q}{(2\pi)^3}\frac{f_0(\widetilde{q}_n^2)[m+b(T,\mu)f_0(\widetilde{q}_n^2)]}{[\widetilde{q}_n^2+(m+b(T,\mu)f_0(\widetilde{q}_n^2))^2]} \;. \tag{7}
$$

Then the propagator is finally read as

$$
G^{-1}(\widetilde{p}_k)=\mathrm{i}\vec{\gamma}\cdot\vec{p}+\mathrm{i}\gamma_4\widetilde{\omega}_k+m+b(T,\mu)f_0(\widetilde{p}_k^2) \;, \tag{8}
$$

and for the free quark propagator

$$
G_0^{-1}(\widetilde{p}_k)=\mathrm{i}\vec{\gamma}\cdot\vec{p}+\mathrm{i}\gamma_4\widetilde{\omega}_k+m \;, \tag{9}
$$

substituting Eq. (8) and Eq. (9) into Eq. (3), we can get

$$
P_{\mathrm{CJT}}(T,\mu)=-2N_{\mathrm{c}}N_{\mathrm{f}}T\sum_{k=-\infty}^{+\infty}\int\frac{\mathrm{d}^3p}{(2\pi)^3}\left[\ln\frac{B(\widetilde{p}_k^2)^2m^2+(B(\widetilde{p}_k^2)^2+m^2)(\vec{p}^2+\widetilde{\omega}_k^2)+(\vec{p}^2+\widetilde{\omega}_k^2)^2}{m^4+2(\vec{p}^2+\widetilde{\omega}_k^2)m^2+(\vec{p}^2+\widetilde{\omega}_k^2)^2}-\frac{B(\widetilde{p}_k^2)(B(\widetilde{p}_k^2)-m)}{\vec{p}^2+\widetilde{\omega}_k^2+B(\widetilde{p}_k^2)^2}\right] \;. \tag{10}
$$

A mathematical equation $\mathrm{tr}(\ln(G^{-1}(\widetilde{p}_k)G_0(\widetilde{p}_k)))=\ln(\mathrm{Det}(G^{-1}(\widetilde{p}_k)G_0(\widetilde{p}_k)))$ is adopted here.

The energy density is obtained as [1]:

$$
\epsilon(T,\mu)=\frac{T^2}{V}\frac{\partial\ln Z(T,\mu)}{\partial T}+\mu\rho=T\frac{\partial P}{\partial T}-P+\mu\rho=T\frac{\partial P_{\mathrm{CJT}}}{\partial T}\Big|_B-P_{\mathrm{CJT}}+\mu\rho+\frac{37\pi^2}{30}T^4+\mu^2T^2-\frac{\mu^4}{2\pi^2}+\mathcal{B} \;. \tag{11}
$$

According to Eq. (10) we have:

$$
T\frac{\partial P_{\mathrm{CJT}}}{\partial T}\Big|_B-P_{\mathrm{CJT}}=-2N_{\mathrm{c}}N_{\mathrm{f}}T^2\sum_{k=-\infty}^{+\infty}\int\frac{\mathrm{d}^3p}{(2\pi)^3}\frac{2\widetilde{\omega}_k\omega_k}{T}\left[\frac{2(m^2-B^2)}{B^2m^2+(B^2+m^2)(\vec{p}^2+\widetilde{\omega}_k^2)+(\vec{p}^2+\widetilde{\omega}_k^2)^2}+\frac{B(B-m)}{(\vec{p}^2+\widetilde{\omega}_k^2+B^2)}\right] \;, \tag{12}
$$

and $\frac{\partial P_{\mathrm{CJT}}}{\partial T}\big|_B$ means $\frac{\partial B}{\partial T}=0$ here. When $G \to G_0$, we get $B \to m$ and $\epsilon \to \epsilon_{\mathrm{free}}$. Otherwise if $\frac{\partial B}{\partial T} \neq 0$, an additional term will appear in the integrand of Eq. (12):

$$\left[\frac{2B(\vec{p}^2+\widetilde{\omega}_k^2+m^2)}{B^2m^2+(B^2+m^2)(\vec{p}^2+\widetilde{\omega}_k^2)+(\vec{p}^2+\widetilde{\omega}_k^2)^2}+\frac{m-2B}{\vec{p}^2+\widetilde{\omega}_k^2+B^2}\right]\frac{\partial B}{\partial T} ,$$
(13)

which destroys the self-consistency of thermodynamics. The quark-number density is [8, 14]:

$$\rho(T,\mu)=(-)N_{\mathrm{c}}N_{\mathrm{f}}T\sum_{i=-\infty}^{+\infty}\int\frac{\mathrm{d}^3p}{(2\pi)^3}\mathrm{tr}_\gamma[G(\widetilde{p}_n)\gamma_4] .$$
(14)

3   Results

In Ref. [16], it is shown that the bag constant $\mathcal{B}$ is quark density dependent ($\mathcal{B}(\rho=0)=400$ MeV/fm^3 and $\mathcal{B}(\rho=\infty)=50$ MeV/fm^3, where ρ is the quark density). Reference [14] proved that when the temperature is zero, the quark density and its chemical potential μ satisfy $\rho \sim \mu^3$. That is to say, $\mathcal{B}$ should reach its maximum when $\mu=0$ and decrease with the increase of μ. For the experiments at RHIC, the corresponding freeze-out temperature T, baryon chemical potential μ_{B} and quark chemical potential μ for $\sqrt{S_{\mathrm{NN}}}=19.6$, 62.4, and 200 GeV are shown in Table 1 (see Ref. [17] for more detail). It can be seen that in relativistic heavy ion collisions μ is comparatively small, and decreases with increasing $\sqrt{S_{\mathrm{NN}}}$.

Table 1.   Correlation between $\sqrt{S_{\mathrm{NN}}}$, temperature, baryon and quark chemical potential.

$\sqrt{S_{\mathrm{NN}}}$/GeV	T/MeV	μ_{B}/MeV	μ/MeV	μ/T_{c}
19.6	159	229	77	0.5
62.4	165	82	28	0.2
200	166	27	9	0.06

The lattice results indicate that the critical temperature T_{c} lies in the range $150-170$ MeV [18]. The value given by the rank-1 separable model is $T_{\mathrm{c}}=150$ MeV [8], which is the value adopted in this paper.

In Fig. 1, using Eq. (3) and Eq. (10), the pressure $P(T,\mu=0)$ normalized by T^4 is shown as a function of T/T_{c}. From top to bottom, the pressure is calculated at $\mathcal{B}=57.5$, 255, and 400 MeV/fm^3 respectively. In the calculation, only u and d quarks are taken into consideration ($N_{\mathrm{c}}=3, N_{\mathrm{f}}=2$). The data points in Fig. 1 come from the results of 2+1 flavor lattice QCD [19].

The parameter $\mathcal{B}=57.5$ MeV/fm^3 comes from Ref. [1], $\mathcal{B}=400$ MeV/fm^3 is the upper limit given by Ref. [16], and $\mathcal{B}=255$ MeV/fm^3 is the value adopted in Ref. [20], in which the QCD EoS is studied with the QGP liquid model. Consistent with the conclusion of Ref. [16] that $\mathcal{B}$ decreases with increasing μ, Fig. 1 shows that, when $\mu=0$, comparing the line with a small bag constant $\mathcal{B}=57.5$ MeV/fm^3, the other two lines with

$\mathcal{B}=255$ MeV/fm^3 and $\mathcal{B}=400$ MeV/fm^3 fit the lattice QCD data better. Since in real relativistic heavy ion collisions the chemical potential μ is small (Table 1), here we adopt $\mathcal{B}=255$ MeV/fm^3, just as in Ref. [20].

In Fig. 2, using Eq. (11) and Eq. (12), $(\epsilon-3P)/T^4$ is shown as a function of T/T_{c} at $\mu=0$. As we have mentioned above, the CJT result is calculated at $\mathcal{B}=255$ MeV/fm^3. The data points in Fig. 2 also come from the results of 2+1 flavor lattice QCD [19].
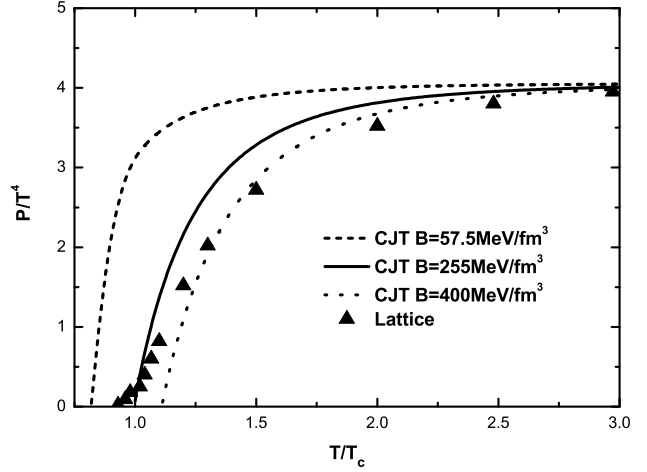
Fig. 1.   The pressure $P(T,\mu=0)$ normalized by T^4 as a function of T/T_{c}, with data points from Ref. [19]. The three lines represent the results at $\mathcal{B}=57.5$, 255, and 400 MeV/fm^3 from top to bottom.
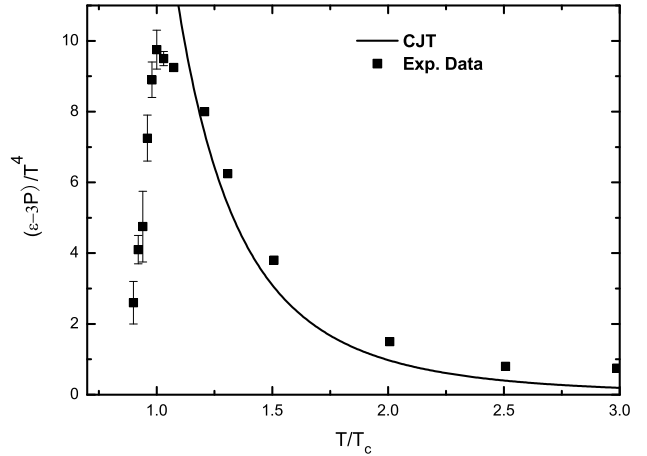
Fig. 2. $(\epsilon-3P)$ normalized by T^4 as a function of T/T_{c} at $\mu=0$, with data points from Ref. [19]. The line represents the CJT results at $\mathcal{B}=255$ MeV/fm^3 .

In the first five plots of Fig. 3, lines show $\Delta P \equiv P(T,\mu)-P(T,\mu=0)$ normalized by T^4 as a function of T/T_{c} for $\mu/T_{\mathrm{c}}=1$, 0.8, 0.6, 0.4 and 0.2. Data points are from Ref. [21] (two-flavor lattice QCD) and Ref. [19] (2+1 flavor lattice QCD). The data of two-flavor lattice
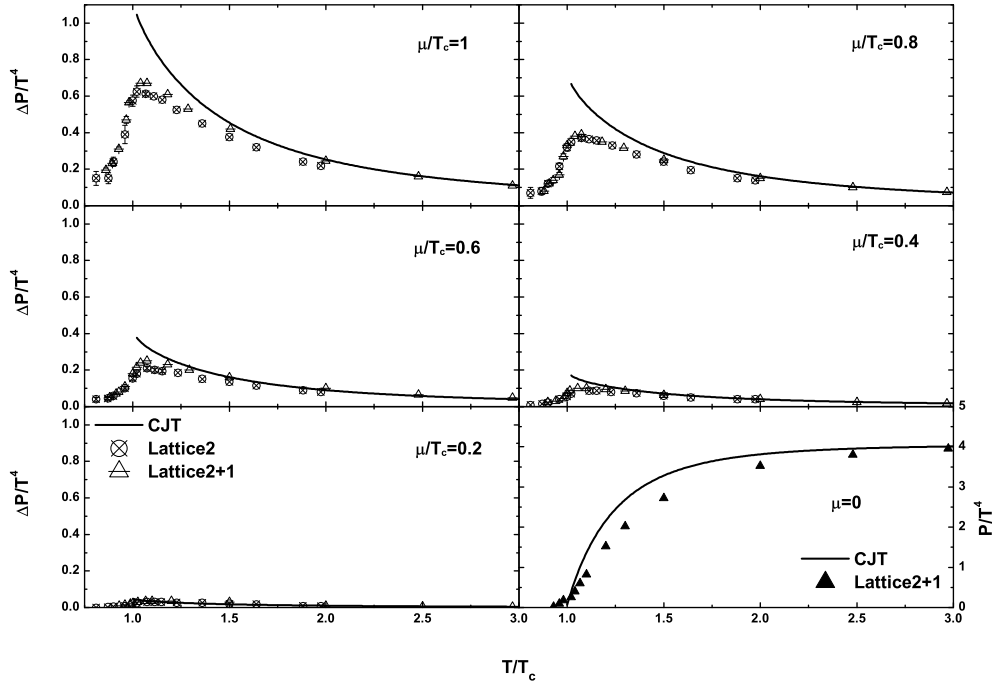
Fig. 3.   For the first five plots, lines are $\Delta P \equiv P(T,\mu) - P(T,\mu=0)$ normalized by T^4 as a function of T/T_c for $\mu/T_c=1$, 0.8, 0.6, 0.4 and 0.2. The data points are from Ref. [21] (lattice2) and Ref. [19] (lattice QCD2+1). For the last plot, the line is the pressure $P(T,\mu=0)$ normalized by T^4 as a function of T/T_c at $\mathcal{B}=255$ MeV/fm^3. The data points are from Ref. [19].
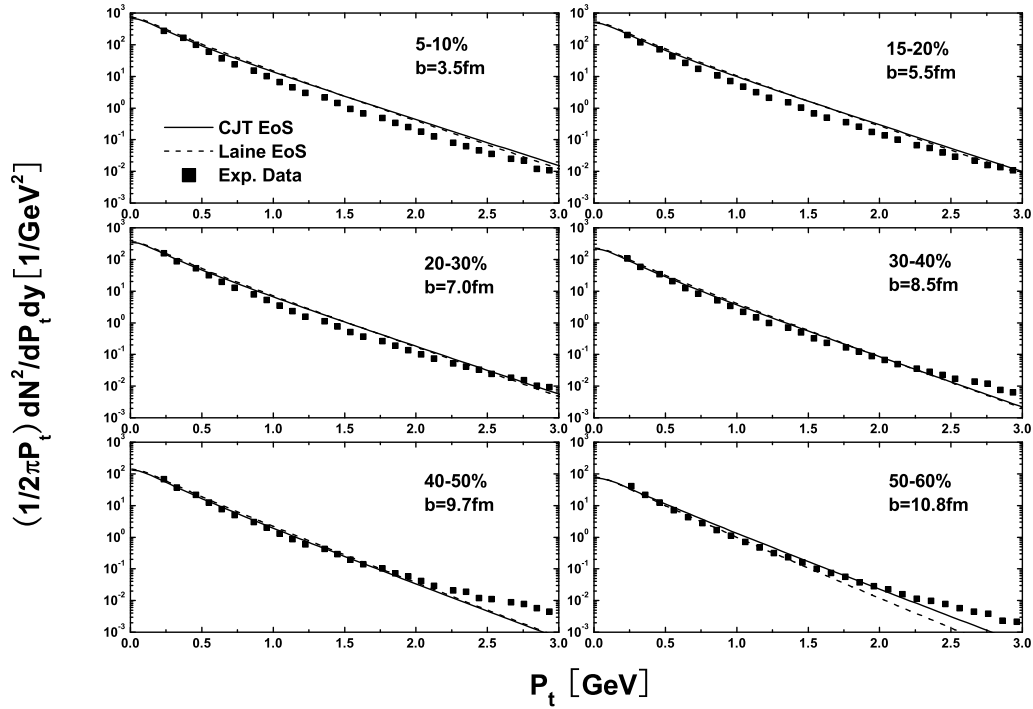
Fig. 4.   The p_T distributions for π^+ in Au+Au collisions at $\sqrt{S_{NN}} = 200$ GeV. The CJT results and the results from Laine's EoS of different impact parameters b are compared with the different centrality bins of the PHENIX data [22].

QCD is for μ/T_c=1, 0.8, 0.6, 0.4 and 0.2 from the first plot to the fifth respectively. The data of 2+1 flavor lattice QCD is for μ_B=530, 410, 330, 210 MeV and 100 MeV respectively, where μ_B is the baryon chemical potential. For the last plot, the line is the pressure $P(T,\mu=0)$ normalized by T^4 as a function of T/T_c at $\mathcal{B}$=255 MeV/fm^3. The data points are from Ref. [19].

In Fig. 2, when $T>1.1T_c$, the CJT result agrees with the lattice QCD data. In Fig. 3, when μ is comparable to T_c (μ/T_c=1 or 0.8), there is deviation from the lattice QCD data for $T\leq1.5T_c$. As μ decreases, the agreement of our result with the lattice QCD data becomes better and better. Considering that real relativistic heavy ion collisions have a small quark chemical potential μ, the CJT results of the QGP EoS agree generally with the lattice QCD data when $T>T_c$. At the same time, all the CJT results in Fig. 2 and Fig. 3 are similar to the results in Ref. [20], in which the QCD EoS was studied using the QGP liquid model: both results generally fit the lattice results well when $T>T_c$ and show deviations from lattice results at and below the T_c region. This region is thought to correspond to the phase transition region or the hadron phase.

We then combine the CJT EoS and the hydrodynamic code UVH2+1 (UVH2+1-0.0beta) [10–13] to obtain two more physics observables, the multiplicity of π^+ mesons produced in heavy ion collisions and the elliptic flows of charged hadrons, and compare them with the experimental results. Since the CJT results of the QCD EoS show deviations from lattice data when $T<T_c$, we adopt the original EoS of the code UVH2+1 in this region. More details of the code UVH2+1 can be found in the Appendix.

The transverse momentum p_T distributions for the produced multiplicity of π^+ in Au+Au collisions at $\sqrt{S_{NN}}$ = 200 GeV are shown in Fig. 4. The different impact parameters b here correspond to the different centrality bins in the RHIC experiments. The data points in Fig. 4 come from the PHENIX group [22]. It is shown that in all centrality bins, when adopting the same initial conditions, our results are almost the same as the results from Laine's EoS [24] (adopted by the original UVH2+1 code) and generally fit the experimental data.

Figure 5 shows the elliptic flows of charged hadrons as a function of transverse momentum p_T for various centrality bins in Au+Au collisions at $\sqrt{S_{NN}}$ = 200 GeV. The CJT results of v_2 are compared with BBC three-subevents method data [23] from PHENIX which is thought to be sensitive to non-flow effects on v_2. It demonstrates that at the impact parameter b= 3.5, 5.5, 7.0 and 8.5 fm, the CJT results are slightly higher than the results with Laine's EoS and are closer to the experimental data. At b=9.7 fm, however, the differences in the two results disappear. Then the results with Laine's EoS exceed the CJT results obviously at b=10.8 fm. Since the differences in the two EoS (CJT and Laine's) only
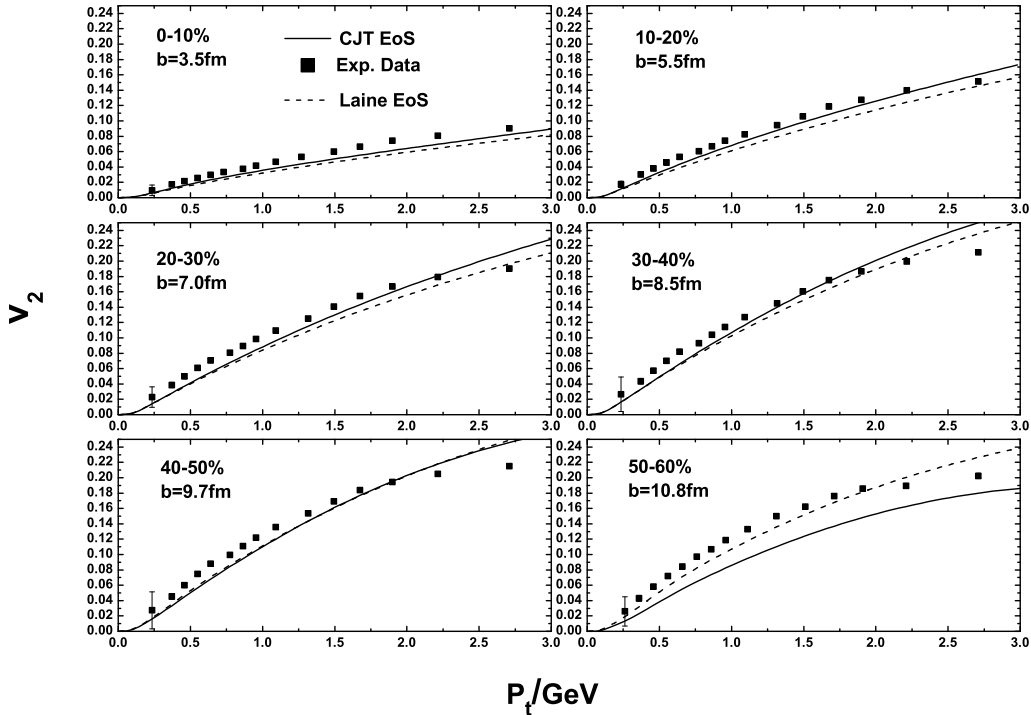
Fig. 5. The elliptic flows v_2 for charged hadrons in Au+Au collisions at $\sqrt{S_{NN}}$= 200 GeV. The CJT results and the results from Laine's EoS of different impact parameters b are compared with the different centrality bins of the PHENIX data [23].

exist at $T>T_c$, it can be concluded that in this region the contribution of the CJT EoS to v_2 is slightly larger than that of Laine's EoS at b=3.5, 5.5, 7.0 and 8.5 fm and obviously smaller than that of Laine's EoS at b=10.8 fm. Because of the asymptotic freedom of QCD, our CJT EoS is more reliable at high temperature. As the impact parameter b increases, however, the high temperature region in QGP reduces. This probably causes the obvious deviation of the CJT results of v_2 from the experimental data at b=10.8 fm.

4   Conclusion

By generalizing CJT effective action to the condition of finite temperature and chemical potential, the pressure of QGP should be obtained from the field theory of QCD. Since CJT effective action is only decided by the quark propagators (free and dressed), using the dressed quark propagator from the rank-1 separable model, we get the EoS of QGP.

The results (P, ΔP and ϵ) from CJT effective action are compared with lattice QCD data in Fig. 1, Fig. 3 and Fig. 2. In Fig. 1, the result of P/T^4 at $\mu=0$ shows that comparing with $\mathcal{B}$=57.5 MeV/fm^3, the larger $\mathcal{B}$ = 255 MeV/fm^3 and $\mathcal{B}$ = 400 MeV/fm^3 fit the lattice QCD data better, which is consistent with the conclusion of Ref. [16]. Considering the real parameters at RHIC, we fix $\mathcal{B}$ at 255 MeV/fm^3, and then we show the results of $\Delta P/T^4$ in Fig. 3 and $(\epsilon-P)/T^4$ in Fig. 2. When μ is small, we find that the CJT results fit the lattice data

[19] for $T>T_c$ and are also similar to the phenomenological model results [20]. At and below T_c, however, there are deviations from the lattice results. We can conclude that the EoS of CJT effective action is reliable at $T>T_c$. We then attempt to use the CJT EoS to study heavy ion collisions. We combine the CJT EoS and the hydrodynamic code UVH2+1 to obtain the multiplicity of π^+ and the elliptic flows of charged hadrons.

Comparing the CJT results of the multiplicity and v_2 with the PHENIX data and the results from the original EoS of Laine and Schröder, we find in Fig. 4 that in all centrality bins the results with our EoS are almost the same as those with Laine's original EoS and generally fit the experimental data. In Fig. 5 it is shown that for impact parameter b=3.5, 5.5, 7.0 and 8.5 fm, the CJT results are slightly larger than those with Laine's original EoS and closer to the experimental data. At b=9.7 fm, however, the differences between the two results disappear. The results with Laine's EoS exceed the CJT results obviously at b=10.8 fm. Because of the asymptotic freedom of QCD, our CJT EoS is more reliable at high temperature. As the impact parameter b increases, however, the high temperature region in QGP reduces. This probably causes the obvious deviation of the CJT results of v_2 from the experimental data at b=10.8 fm.

Comparison of our results with lattice and experimental data and with the results of Laine's EoS suggests that for our next step we should adopt some more complicated DES solutions of the quark propagator to improve the accuracy at low temperature.

Appendix A

The hydrodynamic code UVH2+1 (UVH2+1-0.0beta) is separated into five modules. The first module (initE) produces the initial energy density distribution in the transverse plane and the initial condition is described by the Glauber model, in which energy density is proportional to the number density of binary collisions. The second module (vh2) is the main hydro code, which takes the output from running initE as an input for the energy density and then solves the hydro equations until freeze-out is finished. The third module (convert) converts the hydrodynamic degrees of freedom (energy density, fluid velocities and so on) into particle spectra using the Cooper-Frye freeze-out prescription. The fourth module (reso), which is adapted from the AZHYDRO code, takes the particle spectra and calculates decays of unstable particles using the Particle Data Group values. The fifth module (extract) finally takes the stable particle spectra and calculates the multiplicity, elliptic flow and so on from them.

The influence of EoS is mainly reflected in the first and second module. In the first module (initE) the energy density

distribution is described by the Glauber model:

$$\epsilon(x,y)=\epsilon_0\times n_{\mathrm{bin}}(x,y)\ ,\tag{A1}$$

where n_{bin} is the number density of binary collisions and ϵ_0 is the energy density corresponding to the parameter T_{start}. That is to say, ϵ_0 is EoS related. In order to get the same value of ϵ_0, $T_{\mathrm{start}}=0.362$ GeV in our calculation and $T_{\mathrm{start}}=0.353$ GeV in the original UVH2+1 code. By doing this the two calculations have the same initial conditions.

The other parameters in the two calculations chosen in UVH2+1 are the same: the viscosity over entropy is $\eta/s=$ 0.04, the initial starting time of hydrodynamic description is $\tau_0=1$ fm/c, and the freeze-out temperature is T_{f}=0.150 GeV.

The EoS adopted by the original UVH2+1 is from Laine and Schröder [24]: during the transition region it is determined with lattice simulations, below the transition region it comes from the hadronic resonance gas and above the transition region the phenomenological results for QCD are used. Since the CJT results of the QCD EoS show deviations from lattice data when $T<T_c$, we adopt the original EoS of the code UVH2+1 in this region.

References

1 P.Braun-Munzinger and J. Wambach, Rev. Mod. Phys., **81**: 1031–1050 (2009)
2 J. M. Cornwall, R. Jackiw, and E. Tomboulis, Phys. Rev. D, **10**: 2428 (1974)
3 K. Stam, Phys. Lett. B, **152**: 238 (1985)
4 C. D. Roberts, Sebastian, and M. Schmidt, Prog. Part. Nucl. Phys., **45**: s1 (2000)
5 Y. Hatta and T. Ikeda, Phys. Rev. D, **67**: 014028 (2003)
6 C. Shi, Y. L. Wang, Y. Jiang, Z .F. Cui, and H. S. Zong, JHEP **07**: 014 (2014)
7 D. Blaschke, G. Burau, Yu. L. Kalinovsky, P. Maris, and P. C. Tandy, Int. J. Mod. Phys. A, **16**: 2267 (2001)
8 M. He, J. F. Li, W. M. Sun, and H. S. Zong, Phys. Rev. D, **79**: 036001 (2009)
9 A .M. Zhao, Z. F. Cui, Y. Jiang, and H. S. Zong, Phys. Rev. D, **90**: 114031 (2014)
10 R. Baier, P. Romatschke, and U. A. Wiedemann, Phys. Rev. C, **73**: 064903 (2006)
11 R. Baier and P. Romatschke, Eur. Phys. J. C, **51**: 677 (2007)
12 P. Romatschke, Eur. Phys. J. C, **52**: 203 (2007)
13 P. Romatschke and U. Romatschke, Phys. Rev. Lett., **99**: 172301 (2007)
14 H. S. Zong and W. M. Sun, Phys. Rev. D, **78**: 054001 (2008)
15 C. J. Burden, L. Qian, C. D. Roberts, P. C. Tandy, and M. J. Thomson, Phys. Rev. C, **55**: 2649 (1997)
16 G. F. Burgio, H. Chen, H.-J. Schulze, and G. Taranto, PoS Confinement X, 255 (2013)
17 J. Cleymans, H. Oeschler, K. Redlich, and S. Wheaton, Phys. Rev. C, **73**: 034905 (2006)
18 S. Borsanyi et al, JHEP, **1009**: 073 (2010)
19 Z. Fodor, S. D. Katz, and K. K. Szabo, Phys. Lett. B, **568**: 73–77 (2003)
20 J. Letessier and J. Rafelski, Phys. Rev. C, **67**: 031902 (2003)
21 C. R. Allton, S. Ejiri, S. J. Hands, O. Kaczmarek, F. Karsch, E. Laermann, and C. Schmidt, Phys. Rev. D, **68**: 014507 (2003)
22 The PHENIX Collaboration, Phys. Rev. C, **69**: 034909 (2004)
23 The PHENIX Collaboration, Phys. Rev. C, **80**: 024909 (2009)
24 M. Laine and Y. Schroder, Phys. Rev. D, **73**: 085009 (2006)